ILASS 2008
Sep. 8-10, 2008, Como Lake, Italy

Paper ID ILASS08-3-1

AN EXPERIMENTAL STUDY OF TRANSCRITICAL CO_2 INJECTION

Paul Seebald and Paul E. Sojka

Maurice J. Zucrow Laboratories, School of Mechanical Engineering, Purdue University

ABSTRACT

An experimental study was conducted to investigate the performance of supercritical CO_2 jets injected into a chamber filled with air below the CO_2 critical point. Cone angle, radial concentration profile, and jet penetration length data were collected for swirl numbers (Sn) that ranged from 0.0 to 1.0. They were determined as functions of the swirl number, CO_2 mass flow rate, ratio of CO_2 density to ambient air density, and axial location throughout the jet. Key conclusions drawn from the results are: The radial mass concentration profiles for an injector are similar to each other after normalizing the concentration by the centreline value and the radius by the jet half-radius; cone angles show no dependence on mass flow rate, nor do they vary with changes in Sn—a slight increase was observed for an increase in density ratio; penetration lengths are independent of mass flow rate or density ratio.

INTRODUCTION

Transcritical injection has been given several definitions. The definition adopted here is a supercritical fuel injected into a subcritical environment. To date, very little research has been focused on this type of transcritical injection (TCI).

A supercritical fuel in this case is a fluid where the temperature and pressure are greater than the fuel's thermodynamic critical temperatures and pressures. In this state, there are several noteworthy changes to the fluid physical properties including loss of surface tension and significant variation of density with temperature. The ambient subcritical environment, which in these tests consisted of air, was kept below the critical point of the fuel.

Due to ease of use and safety concerns, carbon dioxide was used as a surrogate for fuel for these experiments. Rachedi [1] showed that carbon dioxide, as tested by Zeaton [2], behaves similarly in supercritical injection to JP-10 and can therefore be used as a substitute fuel.

Transcritical injection has one particular application—aircraft travelling at high-Mach speeds that use gas turbine engines. At speeds greater than Mach 4, the heat generated by the engine and the frame becomes a concern since the surrounding air can no longer be used as a heat sink. As a result, endothermic fuels are being investigated as a possible heat sink. However, heating the fuel prior to injection may cause it to become supercritical, since the pressures in modern gas turbine engine already exceed most fuel critical pressures.

Motivated by these factors, the purpose of this study is to obtain an understanding of how a supercritical fluid behaves when injected into a subcritical environment.

Previous studies considering this type of transcritical injection include Wu [3, 4] and Zong [5]. The former employed injection conditions where P_{inj}/P_{chm} ranged from about 1.7 to 56. These high pressure ratios resulted in Mach disks forming both slightly downstream of the injector and inside of the injector itself, according to Lin [6]. The Mach disks were attributed to a condensation phenomenon similar to homogeneous nucleation. Such a phenomenon is outside the scope of this paper, since the pressure ratios in these tests were less than 1.2, and Lin observed the disappearance of the Mach disk at pressure ratios below 10.

Zong performed a numerical analysis of transcritical injection through a swirl injector, which is the type of injector used here. His analysis considered film thickness and other swirl injector attributes that do not pertain to the present study. However, one of Zong's conclusions was that the cone angle is slightly dependent on mass flow rate.

This study quantitatively explores the effect of density ratio, mass flow rate, and injector geometry on three important characteristics: 1) the radial mass concentration profile, 2) the jet cone angle, or spreading angle, and 3) the jet penetration length. Measurements of temperature and pressure were taken both before injection and after, and the density ratio was calculated based on temperatures and pressures calculated after injection at various axial positions.

In order to make these measurements, a high-speed camera was used to capture images produced by a Schlieren setup. The images were directly affected by refractive index gradients, which could be calculated given the measured temperature and pressure. The images were then analyzed using Matlab codes to extract the three quantities of interest.

The reduced temperature ranged from 0.95 to 1.00, while the reduced pressure varied from 0.94 to 1.00. Minimum and maximum mass flow rates were 2.0 and 3.5 g/s.

Similar to Zong's numerical analysis, swirl injectors were used and characterized by swirl numbers (Sn). Five injectors were tested with swirl numbers of 0.0 (no swirl, straight bore), 0.25, 0.5, 0.75, and 1.0 (high swirl). The present experiments were meant to simplify, but still replicate, the

injection of fuel into a gas turbine engine given transcritical conditions.

EXPERIMENTAL APPARATUS

The TCI experiments were performed at the Combustion Laboratory at Maurice J. Zucrow Laboratories (MJZL), Purdue University. The subsystems are discussed in detail.

Test Vessel

The vessel itself was made from carbon steel tubing and has an inside diameter of 15.2 cm. The injector is attached to a traverse system, which allows images to be taken at various axial positions. Figure 1 shows the setup inside the vessel. Note the quartz observation windows (diameter of 6.35 cm) and honeycomb flow straighteners at the top and bottom of the vessel to ensure 1-d co-flows.

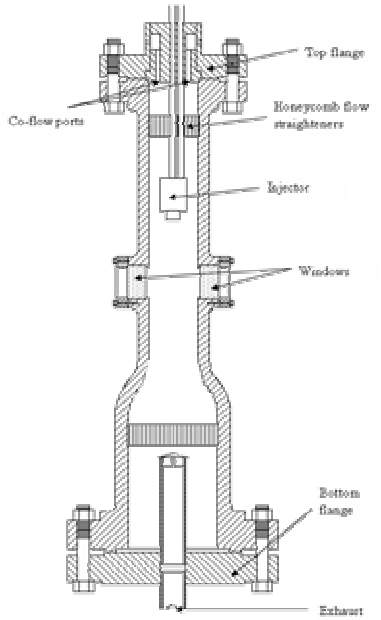

Figure 1: Test Vessel Diagram

A pressure transducer measured the pressure in the vessel, and two thermocouples returned the temperatures of the air co-flow and the injected carbon dioxide, respectively. A thermocouple downstream of the orifice was used to measure the temperature of the flow at the desired axial location.

CO_2 supply

Saturated carbon dioxide was stored in five 22.7 kg cylinders. Gaseous CO_2 drawn from the cylinders went first to a heater, where the temperature was raised above the critical value. It then went through a booster pump, where the pressure was raised to a supercritical value and the mass flow rate controlled. The carbon dioxide then passed through an accumulator to ensure a steady flow rate through the injector. A second heater was used to control the carbon dioxide injection temperature. A Micro-Motion Coriolis-type mass flowmeter was used to directly measure the mass flow rate.

Air Co-Flow Supply

Air was supplied by a 13.8 MPa storage system. It entered the experimental setup at outside temperature, which ranged from about 1 to about 15 C, so it was heated before entering the vessel. The flow rate was obtained using a Micro-Motion Coriolis-type mass flowmeter.

Data Acquisition

Druck pressure transducers and Omega Type-E thermocouples were used for data measurements. National Instruments SCXI data hardware was employed, as was Labview software. A Labview program controlled valves and heaters, and monitored the data.

Injector Design

The pressure-swirl atomizer design is identical to that used by Zeaton in his supercritical study. The three main parts are a plenum, a swirl insert and an orifice plate. Different swirl inserts were made in order to vary the swirl number.

The Syred *et al* [7] definition of swirl number was used:

$$Sn = \frac{\pi d_0^{\,2}}{4A_p} \qquad (1)$$

It is essentially a measure of radial momentum to axial momentum. The diameter of the exit orifice was set at 1.0 mm.

Schlieren Optical System

The Schlieren setup was also used by Rachedi and Zeaton, and was originally designed by Settles [8]. It can be seen in Fig. 2.

Light generated by a theatre lamp was focused on to one end of a fiber-optic cable by a condenser lens. The other end of the fiber-optic cable led to a rectangular slit. Light exiting the slit impinged on a parabolic mirror tilted at about 3°, then entered the vessel.

After passing through the vessel the light was incident on a second mirror, also tilted at 3° but in the opposite direction of the first one. The light beam was then disrupted by a knife edge (cutoff 50%), and directed onto a white screen. A high-speed camera captured the resulting image.

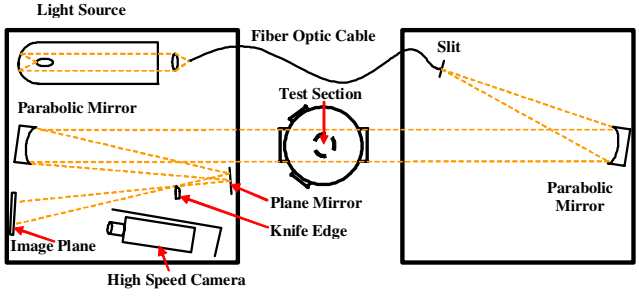

Figure 2: Schlieren System Setup

RESULTS AND DISCUSSION

Obtaining mass concentration profiles from the schlieren images was achieved using a Schardin approximation and Keagy and Ellis s [9] method. Images were taken at axial positions of x/d_0 = 20, 40, and 60.

The radial concentration profiles were plotted using concentration normalized by the centerline value. The radius was normalized by the jet half-radius, with jet half-radius defined as the location where the mass concentration fell to half of the centerline value. Both Zeaton and Rachedi observed that by normalizing the concentration profiles in this manner, the profiles generally fell onto similar curves.

The concentration profiles for the axial positions of x/d_0 = 20, 40, and 60 for each swirl injector (except Sn = 0.0, which has data at x/d_0 = 40, 60, and 80) are shown in Figs. 3 through 7. All profiles are at approximately the same density ratio and mass flow rate.

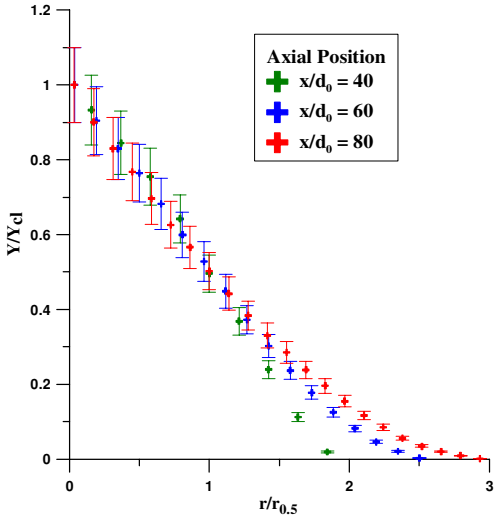

Figure 3: Normalized concentration versus normalized radius for a swirl number of 0.0, density ratio of 9.6, and mass flow rate = 2.5 g/s

Figure 3 shows that the mass profiles for the 0.0 swirl number look similar to each other. Concentration plots for Sn = 0.0 at x/d_0 = 20 were too dense to properly analyze. Figures 4 through 7 show that the mass concentration plots for the other swirl numbers are also similar to within experimental uncertainty.

Figures 4 through 7 also show that the non-zero swirl number profiles have an offset peak. The Sn = 0.25 data show this behavior most clearly. This is clearly different from the supercritical profiles observed by Rachedi and Zeaton.

Since the normalized centerline concentration seems to increase with radial distance at the lower x/d_0 values, it would appear that the swirling action initially drives the CO_2 radially outward and that turbulent mixing then takes over. The higher swirl number cases (Sn = 0.75, 1.0) may not exhibit this behavior because of vortex breakdown, which would explain higher concentrations toward the middle of the jet.

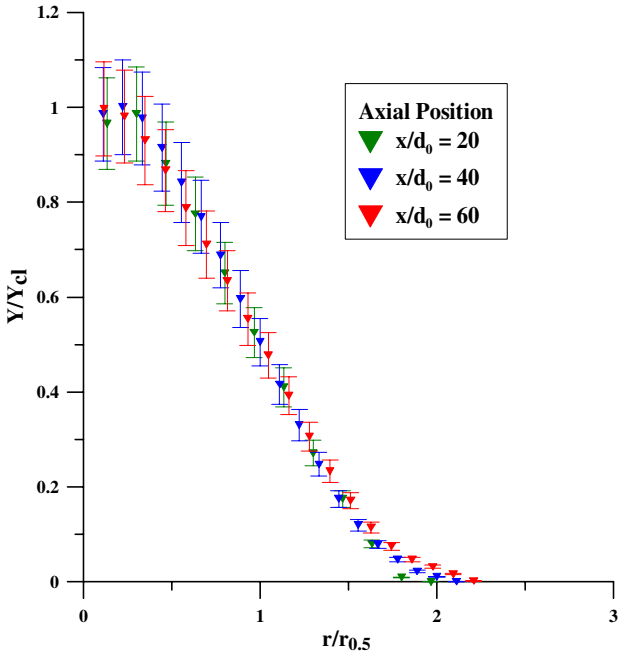

Figure 4: Normalized concentration versus normalized radius for a swirl number of 0.25, density ratio of 9.5, and mass flow rate = 3.0 g/s

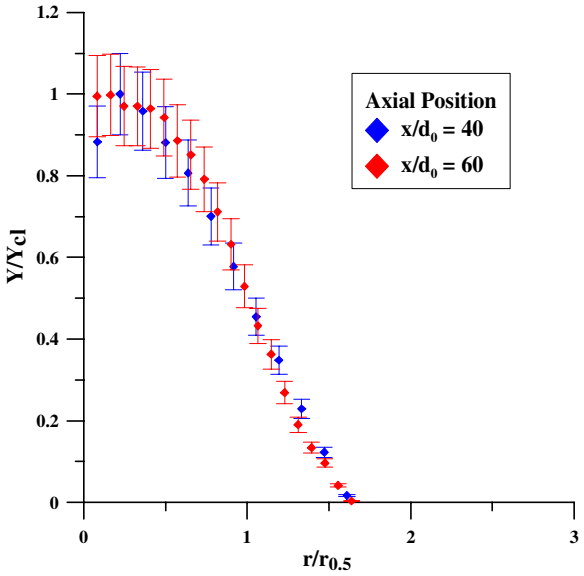

Figure 5: Normalized concentration versus normalized radius for a swirl number of 0.50, density ratio of 9.5, and mass flow rate = 2.7 g/s

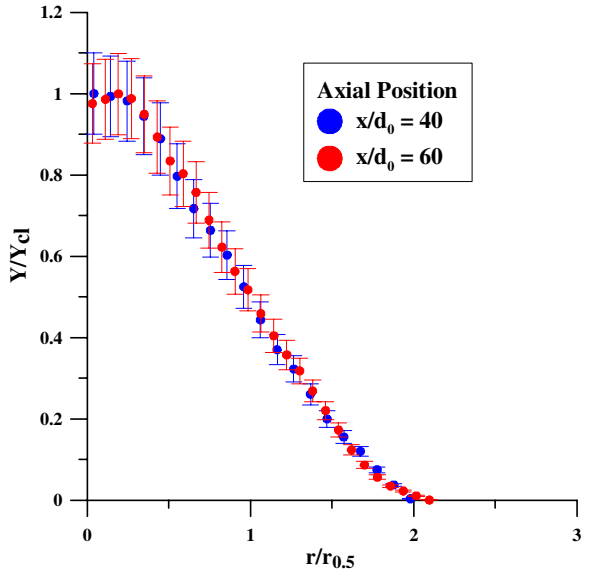

Figure 6: Normalized concentration versus normalized radius for a swirl number of 0.75, density ratio of 9.7, and mass flow rate = 3.2 g/s

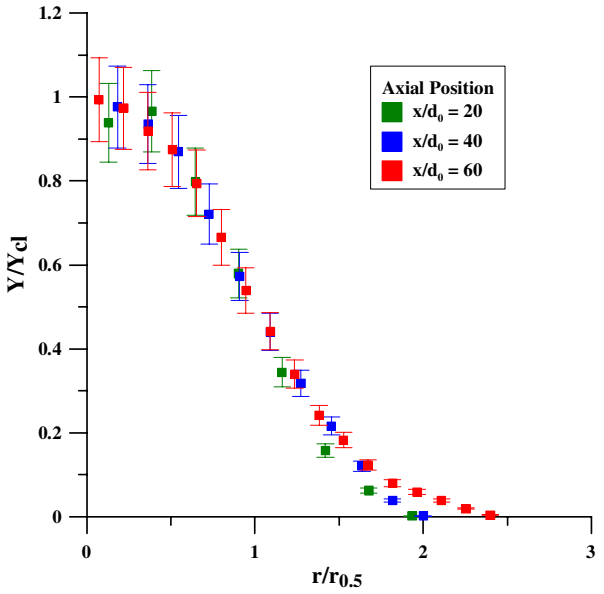

Figure 7: Normalized concentration versus normalized radius for a swirl number of 1.0, density ratio of 9.75, and mass flow rate of 2.2 g/s

Figures 8 and 9 show how mass concentration profiles vary with density ratio and mass flow rate, respectively. Figure 8 contains concentration profiles for Sn = 0.25 at x/d_0 = 20, where the mass flow rates are approximately equal and the density ratio varies. Figure 9 contains concentration profiles for Sn = 0.50 at x/d_0 = 40, where the density ratios are approximately equal and the mass flow rate varies. Both figures are representative of the all data collected data.

Figure 8 shows a slight dependency on density ratio: as density ratio increases, the concentration profiles widen slightly. Figure 9 indicates that radial mass concentration profiles are independent of mass flow rate.

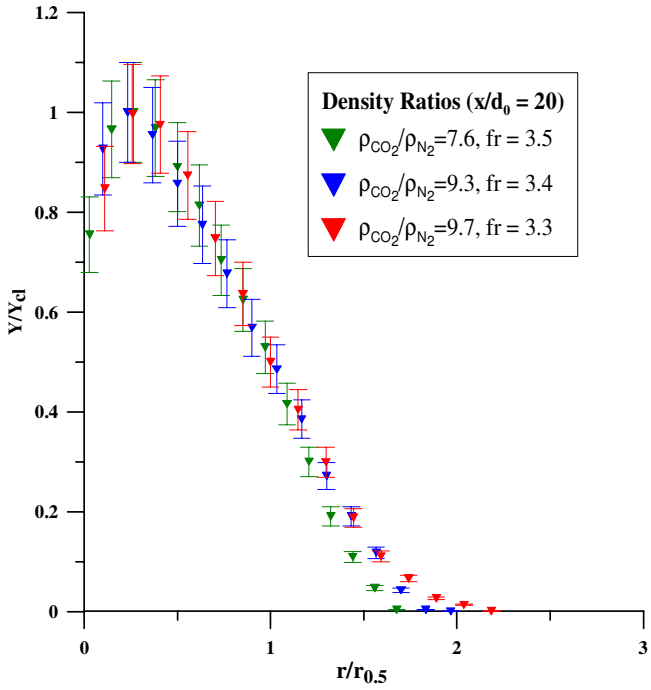

Figure 8: Normalized concentration versus normalized radius for a swirl number of 0.25, mass flow rate of ≈ 3.4, and three density ratios

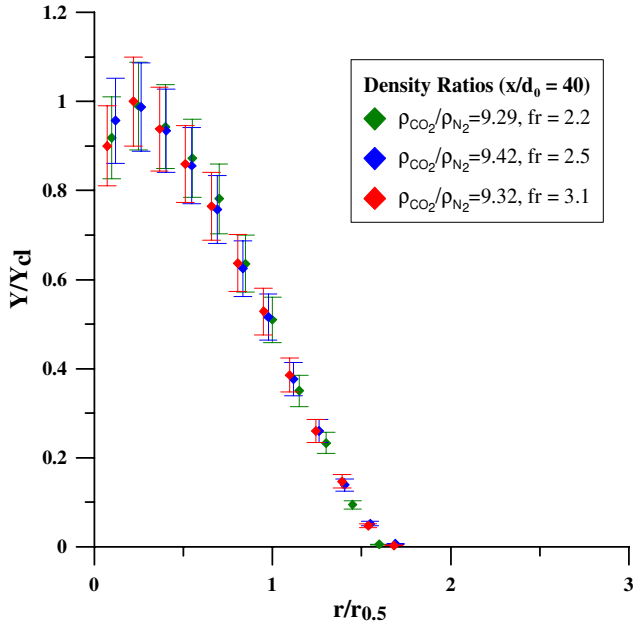

Figure 9: Normalized concentration versus normalized radius for a swirl number of 0.50, density ratio of ≈ 9.3, and three values of mass flow rate (fr)

Cone angle measurements were also made at each axial position for various density ratios and mass flow rates. The full cone angle is defined by Eq. (2), where l represents the the axial position relative to the orifice, and h stands for the half-width of the jet at that axial location:

$$\tan\frac{\theta}{2}=\frac{l}{h} \qquad (2)$$

Figures 10 through 14 show cone angles for each swirl number. Note that neither density ratio nor mass flow rate has a significant effect on cone angle (within experimental uncertainty), at least for the density ratios considered here.

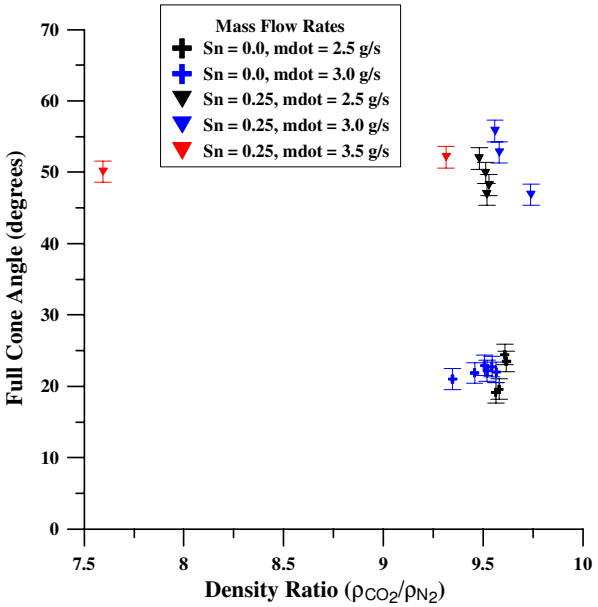

Figure 10: Full cone angle versus density ratio for swirl numbers of 0.0 and 0.25, $x/d_0 = 20$

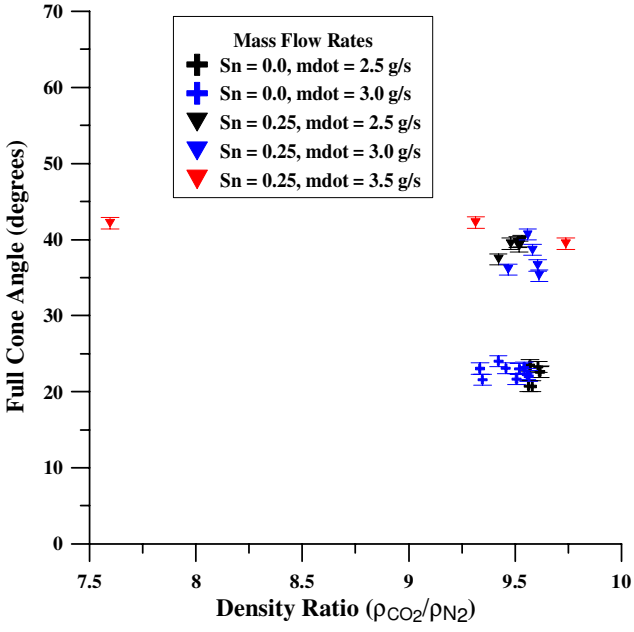

Figure 11: Full cone angle versus density ratio for swirl numbers of 0.0 and 0.25 and $x/d_0 = 40$

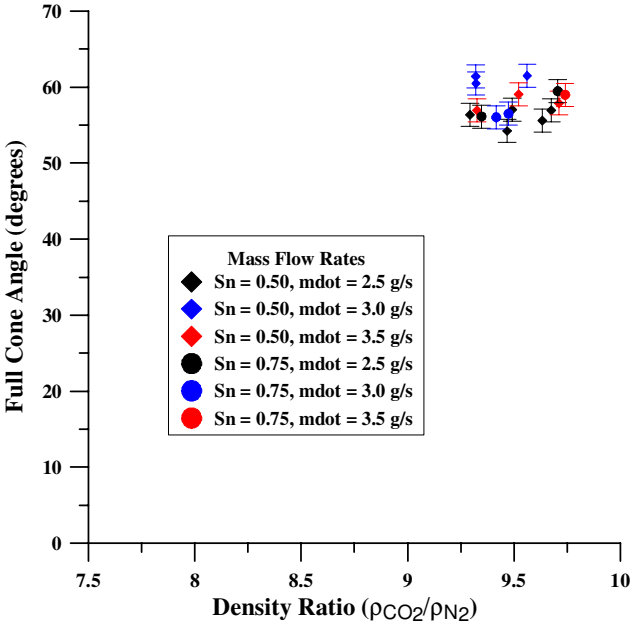

Figure 12: Full cone angle versus density ratio for swirl numbers of 0.50 and 0.75 and $x/d_0 = 20$

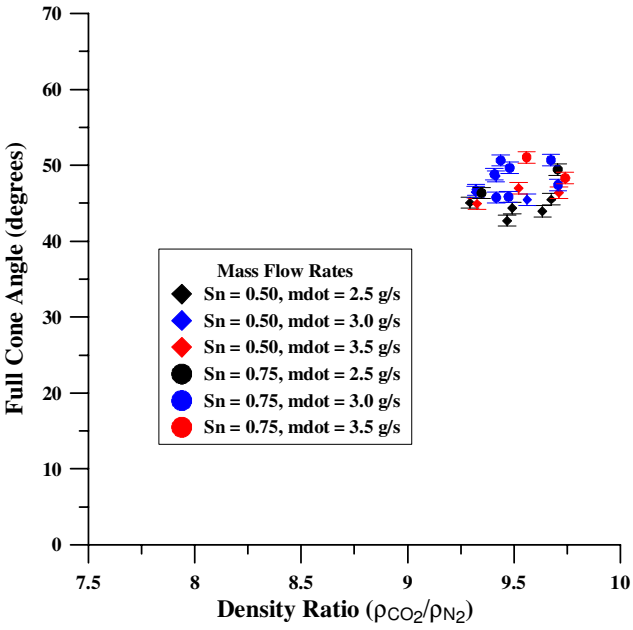

Figure 13: Full cone angle versus density ratio for swirl numbers of 0.50 and 0.75, and $x/d_0 = 40$

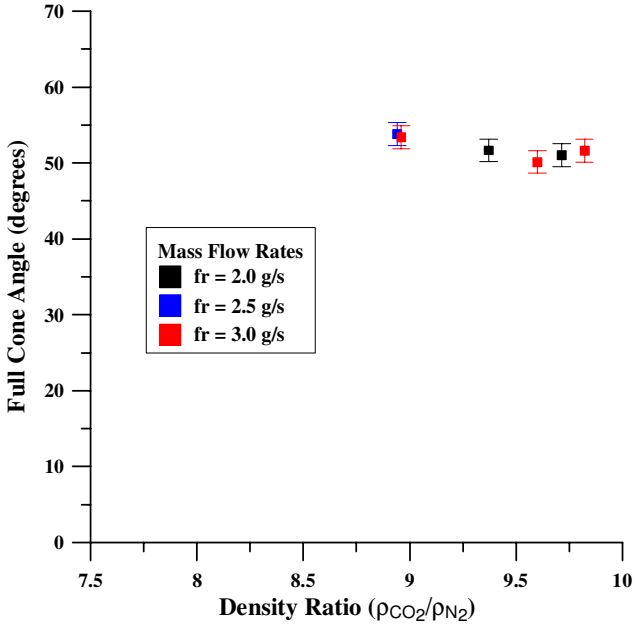

Figure 14: Full cone angle versus density ratio for a swirl number of 1.0 and $x/d_0 = 20$

Figure 15 presents cone angles at $x/d_0 = 20$ for each swirl case. There is little difference between the Sn = 0.5 and Sn = 0.75 cone angles, and the Sn = 1.0 cone angles are actually less than those two. This is surprising since initial cone angle was expected to be controlled by injector internal geometry, as shown by [1,2]. This topic warrants further investigation.

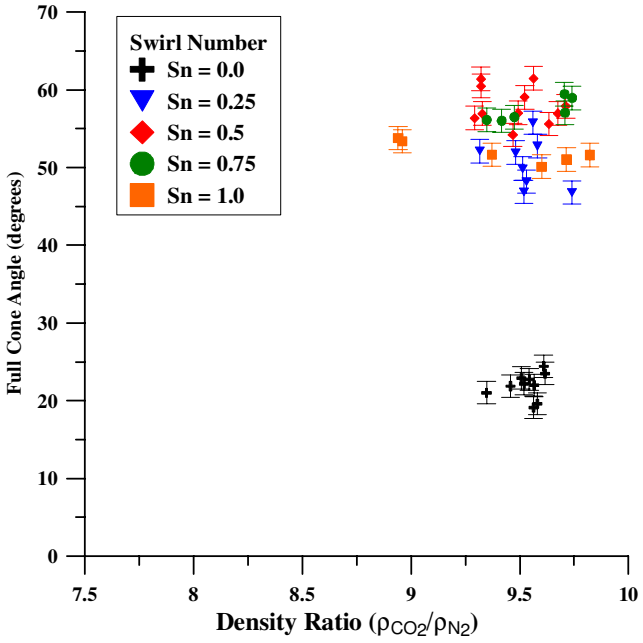

Figure 15: Full cone angle versus density ratio, variation with swirl number for $x/d_0 = 20$

Table 1 lists average cone angles for each swirl number at various axial positions ($x/d_0 = 20$, 40, and 60), along with the corresponding standard deviations. The data show that cone angles decrease as downstream distance increases, for all swirl numbers above zero. This was also observed to occur in supercritical jets [1,2], and can be attributed to entrainment of air which drives the CO_2 inward . The effect is probably too small to observe when Sn=0.0

Table 1: Average full cone angles (degrees)

	Axial Location		
Sn	$x/d_0 = 20$	40	60
0.0	22±2	22±1	22±1
0.25	50±3	39±2	34±2
0.50	58±2	46±2	39±1
0.75	57±2	49±2	43±2
1.0	52±1	46±2	42±1

Penetration length was also measured for each swirl number case. Penetration length is defined here as the distance from the orifice where the centerline concentration is 20% of the centerline concentration at $x/d_0 = 20$. There is no penetration length data for Sn = 0.0 because the concentration data could not be analyzed for that case.

The results of the penetration length analysis are shown in Fig. 16, where the data are sorted by swirl injector. Figure 17 shows the variation of penetration length with changes in mass flow rate and density ratio.

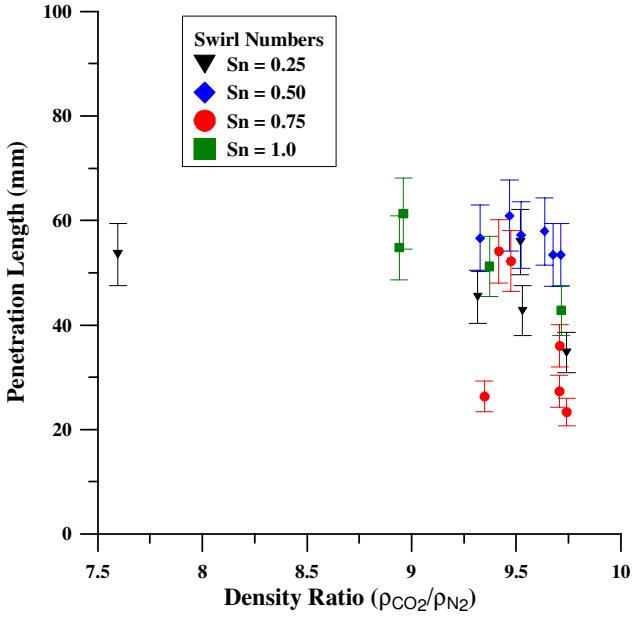

Figure 16: Penetration length versus density ratio, variation with swirl number

Figure 17 indicates that penetration length is not dependent on mass flow rate or density ratio for the range of flow rates employed, at least to within the experimental uncertainty. This is in contrast to the work of both Rachedi and Zeaton, who saw dependencies of the penetration length on mass flow rate and density ratio in supercritical jets. Perhaps a larger range of mass flow rates would reveal different trends.

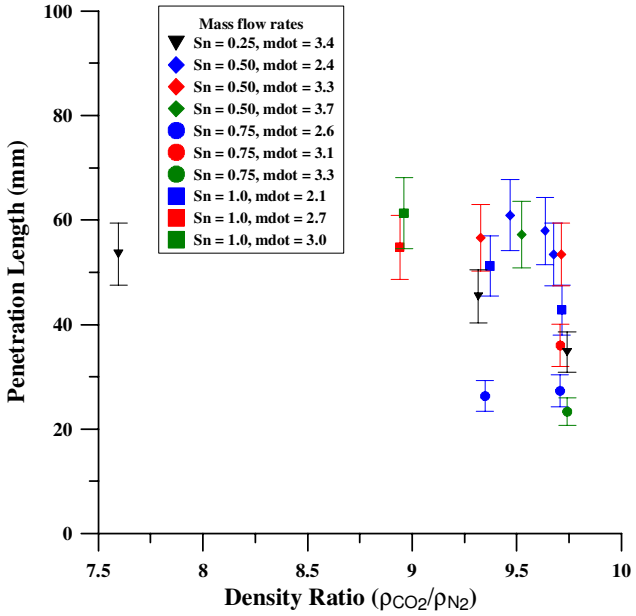

Figure 17: Penetration length versus density ratio, variation with swirl number and mass flow rate

CONCLUSIONS

Mass concentration profiles, cone angles and penetration lengths were measured for transcritical CO_2 injection through swirl injectors having Sn of 0.0, 0.25, 0.50, 0.75, and 1.0. Density ratio, mass flow rate, and swirl number were varied. The following conclusions were drawn:

1. The radial mass concentration profiles for an injector are similar to each other after normalizing the concentration by the centreline value and the radius by the jet half-radius.
2. The mass concentration profiles show no dependence on mass flow rate, but widen slightly as density ratio increases.
3. The cone angle data do not show a dependence on mass flow rate or density ratio.
4. The cone angles did not demonstrate the expected increase with an increase in swirl number. At $x/d_0 = 20$, both Sn = 0.50 and 0.75 cone angles are greater than Sn = 1.0 full cone angles.
5. Cone angles decreased with axial position, as expected, except for Sn = 0.0 which had an almost constant full cone angle at all axial positions. This is attributed to entrainment of surrounding air into the jet.
6. Penetration length does not show a dependence on mass flow rate or density ratio.

NOMENCLATURE

Symbol	Quantity	SI Unit
A_p	Area of ports	mm^2
d_0	Orifice diameter	mm
dr	Density ratio	dimensionless
h	Half-height of jet	mm
l	Axial distance	mm
mdot	Mass flow rate	g/s
P	Pressure	MPa
P_{chm}	Chamber pressure	MPa
P_{inj}	Injection pressure	MPa
r	Radius	mm
$r_{0.5}$	Jet half-radius	mm
Sn	Swirl number	dimensionless
x	Axial position	mm
Y	Mass concentration	g
Y_{cl}	Centerline concentration	g
ρ	Density	g/m^3
θ	Jet cone angle	degrees

REFERENCES

[1] R. Rachedi *et al*., An Experimental Study of Swirling, Supercritical Hydro-carbon Fuel Jets, *ASME Journal for Gas Turbines and Power*, accepted (2008).

[2] G. Zeaton *et al*., An Experimental Study of Supercritical Fluid Jets, *ASME Journal for Gas Turbines and Power*, submitted (2008).

[3] P. Wu and T. Chen, Injection of Supercritical Ethylene in Nitrogen, *Journal of Propulsion and Power*, vol. 12, no. 4, pp. 770-777, 1996.

[4] P. Wu *et al*, Expansion and Mixing Processes of Underexpanded Supercritical Fuel Jets Injected into Superheated Conditions, *Journal of Propulsion and Power*, vol. 15, no. 5, pp. 642-649, 1999.

[5] N. Zong and V. Yang, Dynamics of Simplex Swirl Injectors for Cryogenic Propellants at Supercritical Conditions, 42nd AIAA Aerospace Sciences Meeting and Exhibit, AIAA 2004-1322, 2004.

[6] K.-C. Lin and S. Cox-Stouffer, Structures and Phase Transition Processes of Supercritical Methane/Ethlyene Mixtures Injected into a Subcritical Environment, *Combust. Sci. And Tech.*, vol. 178, pp. 129-160, 2006.

[7] N. Syred *et al.*, Temperature and Density Gradient Changes Arising with the Precessing Vortex Core and Vortex Breakdown in Swirl Burners, *15th Symposium (International) on Combustion*, pp. 587-597, 1974.

[8] G. Settles, Schlieren and Shadowgraph Techniques, Springer, New York, 2001.

[9] W. Keagy and H. Ellis, The Application of the Schlieren Method to the Quantitative Measurement of Mixing Gases in Jets, *3rd Symposium on Combustion and and Flame and Explosion Phenomena*, pp. 667-674, 1949.